Enhanced Spatial Localization of Neuronal Activation Using Simultaneous Apparent-Diffusion-Coefficient and Blood-Oxygenation Functional Magnetic Resonance Imaging

Allen W. Song, Marty G. Woldorff, Stacey Gangstead, George R. Mangun, and Gregory McCarthy

Brain Imaging and Analysis Center and Center for Cognitive Neuroscience, Duke University, Durham, North Carolina 27710

Functional MRI (fMRI) can detect blood oxygenation level dependent (BOLD) hemodynamic responses secondary to local neuronal activity. The most commonly used method for detecting fMRI signals is the gradient-echo echo-planar imaging (EPI) technique because of its sensitivity and speed. However, it is known that much of the signal obtained with this approach arises from large veins, with additional contribution from the capillaries and venules. Early experiments using diffusion-weighted gradient-echo EPI have suggested that intravoxel incoherent motion (IVIM) weighting can selectively attenuate contributions from large vessels based on the differences in the mobility of the blood within them, thereby revealing the contributions from hemodynamic changes in capillaries, which are in close spatial proximity to the activated neural tissue. Using this differential sensitivity of the various neurovascular compartments to IVIM weighting, we present a new approach for deriving functional maps of neural activity. This method is based on task-induced changes of the apparent diffusion coefficients (ADC), a signal that we demonstrate is generated in vascular compartments that only partially overlap with those generating the BOLD signal. The approach allows both the ADC-based maps and the more commonly used BOLD-based maps to be acquired simultaneously. The spatial overlap between these maps can be used to create composite maps that permit improved localization of the underlying neuronal activity patterns by identifying signals generated in those vascular components that are in closest proximity to the active neuronal populations of interest. © 2002 Elsevier Science (USA)

Key Words: **fMRI; BOLD; ADC; IVIM; diffusion weighting.**

INTRODUCTION

The development of functional magnetic resonance imaging (fMRI) (Belliveau *et al.,* 1991; Kwong *et al.,* 1992; Bandettini *et al.,* 1992; Ogawa *et al.,* 1992; Menon *et al.,* 1993; Turner *et al.,* 1993) has given neuroscientists a powerful tool to noninvasively map neuronal activity. Local changes in blood oxygenation level are triggered by neuronal activity and thus are generally believed to provide a good spatial measure of the location of the activated brain areas. However, the blood oxygenation level dependent (BOLD) (Ogawa *et al.,* 1993) changes that are detected with fMRI can arise from various vascular networks. Some of these vascular areas are in close spatial proximity to the neuronal activity of interest (e.g., capillaries), but some can be relatively distant, such as the large draining veins. This poses a serious problem for the spatial resolution of fMRI for mapping neural activity.

In order to improve the localizing capability of fMRI, it is crucial to distinguish between the various sources contributing to the BOLD signals. Previous studies have indicated that methods such as diffusion weighting can be used to suppress signals from larger vessels while minimally impacting signals generated in capillaries, thereby providing some improvement in spatial localization of neuronal activity (Song *et al.,* 1996; Boxerman *et al.,* 1995; Zhong *et al.,* 1998). In these studies, rather moderate diffusion weighting was used thus resulting in, effectively, the intravoxel incoherent motion (IVIM) weighting (Le Bihan *et al.,* 1986; Le Bihan and Turner, 1992) originally proposed by Le Bihan *et al.* However, it has been difficult to correlate the amount of IVIM weighting with the size of vessels that are being affected. As a result, the use of simple IVIM weighted protocols for attenuating unwanted signals (i.e., those generated at sites relatively distant from the neuronal activity) may not result in the attenuation of those signals with sufficient strength or selectivity. The general methodology of diffusion weighting was also used in recent studies (Does *et al.,* 1999; Zhong *et al.,* 1991) to investigate the contribution of background gradients. It was found that apparent diffusion coefficients (ADC) of the extravascular tissue were dependent on intravascular susceptibility, suggesting the potential use of intermediate diffusion

weighting in fMRI to investigate the ADC changes of brain tissue. A most recent study (Darquie *et al.,* 2001) investigated true diffusion effects with very strong diffusion weighting, reporting changes of diffusion properties related to the cellular volume changes. These studies suggested that the general methodology of diffusion weighting can be used to investigate the mobility changes of intravascular proton pools and extravascular tissues, and even at the cellular level.

The present study aims to study intravascular ADC changes using IVIM weighting and to compare these changes with those of the BOLD contrast. Such an investigation is made possible by using a dynamically ramped IVIM weighting method that allows simultaneous acquisition of the time courses based on the BOLD as well as the ADC contrast. While the functional signal based on the BOLD contrast is generally accepted to have arisen from capillaries plus the venous network, (Ogawa *et al.,* 1993), the activation based on the ADC contrast, because of its apparent sensitivity to mobility changes, is believed to be generated in the vascular networks that experience flow changes (Song and Popp, 1998; Darquie *et al.,* 1999; Song *et al.,* 2000). Since large arteries usually have turbulent flows and large veins do not experience significant flow changes under normal physiological conditions (Guyton *et al.,* 2000), these networks would include small arterial networks, the capillaries, and, possibly, small venules. The combined information from the ADC-based and BOLD-based maps can be used to identify the vascular origins of the functional MRI signals. Moreover, the activated areas that overlap from these two maps reveal the signals that arise from the smaller vessels and capillary beds that are in close spatial proximity to the active neurons, thereby improving the spatial localization of functional neuronal activity.

THEORETICAL FRAMEWORK

It is well known that diffusion weighting can be used to selectively attenuate MR signals from proton pools undergoing random-walk diffusion process (Torrey, 1956). The signal attenuation factor *F,* defined as the ratio of the signal after attenuation to the original signal, is governed by the equation

$$F = e^{-\int_0^T \mathbf{k}(t) \cdot \mathbf{D} \cdot \mathbf{k}(t) dt}, \qquad (1)$$

where $\mathbf{k}(t) = \int_0^T \gamma \mathbf{G}(t') dt'$ is the *k*-space trajectory, $\mathbf{D}$ is the diffusion tensor, *g* is the gyromagnetic ratio (for proton, it is $2\pi * 42.58 \times 10^6$ rad/T), and $\mathbf{G}(t)$ is the gradient vector used to generate diffusion weighting. If the gradient waveforms ($\mathbf{G}_x(t)$, $\mathbf{G}_y(t)$, and $\mathbf{G}_z(t)$) used at *x, y,* and *z* directions are orthogonal to each other, which is incorporated into our design, then the off

diagonal elements of the diffusion tensor dot do not sustain any weighting, resulting in a scalar representation of Eq. (1) as

$$F = e^{-(D_{xx}\int_0^T (\gamma G_x)^2 dt + D_{yy}\int_0^T (\gamma G_y)^2 dt + D_{zz}\int_0^T (\gamma G_z)^2 dt)}. \qquad (2)$$

By forcing $\int_0^T (\gamma G_x)^2 = \int_0^T (\gamma G_y)^2 = \int_0^T (\gamma G_z)^2 = \frac{b}{3}$ in our gradient design, Eq. (2) can be further simplified to become

$$F = e^{-bD}, \qquad (3)$$

where *D* is the trace of the diffusion tensor, defined by $(D_{xx} + D_{yy} + D_{zz})/3$, which is rotationally invariant, and *b* is the weighting factor that is used in the image acquisition protocol. From Eq. (3), it can be seen that the bigger the *D* and the *b* factors, the larger the attenuation.

For randomly oriented blood vessels within the voxel, the original random-walk theory of the diffusion process is not appropriate because the motion pathway is no longer truly stochastic. However, the signal attenuation is still present and can be analyzed using the theory of the IVIM (Le Bihan *et al.,* 1986; Le Bihan and Turner, 1992). Le Bihan *et al.* (1988) discussed in detail two models to analyze the attenuation effects due to random flows: one assumed that flows change directions within the echo time, and the other assumed no change of directions. Under a short echo time (<50 ms) used in our gradient-echo spiral imaging sequence, we adopted the latter model and assumed that the flows do not change directions during this period. Because the IVIM gradient waveforms in our experiments have an inherent zero-flow moment along one dimension, this flow model can be reduced to a two-dimensional process. Under these conditions, the attenuation factor *F* of these flow segments, which is the spatial integration of all the flow signals under IVIM weighting, is governed by

$$F = \left| \int_0^{2\pi} \frac{f}{2\pi} \cdot e^{jcv\cos\theta} d\theta \right| = |f \cdot J_0(cv)|, \qquad (4)$$

where $c = \gamma \int_0^T G(t) \cdot t \cdot dt$, $G(t)$ is the gradient waveform used for IVIM weighting, *f* is the volume fraction of the vessels, *v* the velocity of blood flow, θ the angle between each flow segment and the flow-sensitized direction of the IVIM weighting gradient, and J_0 the Bessel function of the first kind. Since the magnitude information is acquired during image acquisition, the absolute values of J_0 would reflect the detected signal and are plotted in Fig. 1 for $c \cdot v$ from 0 to 6. Thus the combined attenuation factor, including the surrounding brain tissue undergoing normal diffusion process, is
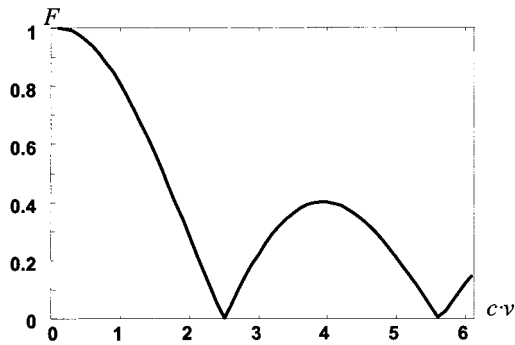
FIG. 1. Absolute values of Bessel function of the first kind, J_0 $(c \cdot v)$ for $c \cdot v$ from 0 to 6.

$$F = |f \cdot J_0(cv) + (1 - f) \cdot e^{-bD}|, \qquad (5)$$

where b is the inherent diffusion weighting factor, and D is the diffusion coefficient of the brain tissue. The additional term simply describes the attenuation of the normal brain tissue of volume fraction $(1 - f)$ times the typical exponential decay function seen under diffusion weighting.

While the IVIM weighting gradients in our experiments have flow moment nulled along the trans-plane dimension, the in-plane flow is present and determines the value of c; in our experiments, as calculated from the definition noted above, $c = 0.76$ rad s/mm. Since the overall signal attenuation is governed by both f and J_0, attenuation was analyzed under the following two possible conditions: (1) f (i.e., the vessel volume fraction) increases as blood flow increases and (2) f remains the same as blood flow increases. Under Condition 1, the overall signal will be more attenuated when the vessel volume fraction f increases (i.e., the larger the f, the smaller the F), provided that $e^{-bD} > J_0(c \cdot v)$. This is true in the present study, because D is ~0.6×10^{-3} mm²/s, and b is kept <229 s/mm², so that e^{-bD} is >0.88, and since generally $v > 1$ mm/s (Zhong et al., 1991), so that $c \cdot v > 0.76$ and $J_0(c \cdot v) < 0.86$. As a result, when blood flow increases, the overall signal would decrease; if this combined process is fit using Eq. (3), apparent diffusion coefficient - ADC can be obtained and would show an increase in value, thus leading to a positive activation in ADC-based images. Under Condition 2, the term $J_0(c \cdot v)$ dominates the signal changes, so F will follow its pattern. Depending upon the value of $(1 - f) \cdot e^{-bd}$, F in Eq. (5) may have the transition point when $c \cdot v = T$, where T is between 2.4 (the transition point of $|J_0(c \cdot v)|$) and 3.8 (the transition point of $J_0(c \cdot v)$). A positive correlation between the blood flow velocity and signal attenuation is maintained when $c \cdot v < T$, or when $v < 1.32 T$ (3.2 to 5.0) mm/s. That is, an increase of velocity would correspond to a more significant signal attenuation (i.e., smaller F) and higher ADC, which would then be reflected by a positive activation in the ADC contrast. Since these flows

have low velocities and show changes during activation, they would likely be within very small vessels and capillaries. For higher velocities, such as would exist in larger vessels that are likely to be relatively *distant* from the neuronal activities, an opposite correlation would occur. That is, an increase of velocity would correspond to a less significant signal attenuation and lower ADC, which would then lead to the negative signal change in the ADC contrast.

For vessels that do not have a random distribution within the voxel, which tends to be the larger vessels such as arteries and veins, the fluid dynamics are more complex. However, previous reports have indicated that these signals are quickly attenuated even in the presence of very small diffusion weighting, due to the significant intravoxel dephasing from the diverse velocity profiles common in these vessels with large diameters (Song et al., 1996; Boxerman et al., 1995; Zhong et al., 1998). Thus, large arteries and veins do not significantly contribute to the ADC contrast in our experiments. It should be noted, however, that large veins *do* contribute significantly to the BOLD contrast.

To this end, it can be inferred that ADC contrast mainly arises from the small arteries, arterioles, capillaries, and venules, compared to the BOLD contrast, which mostly originates from the veins, venules, and capillaries. Given that these two contrast mechanisms have partially distinct vascular sensitivity with limited spatial overlap, any colocalization between BOLD and ADC signals during activation would therefore reflect signals arising in capillaries and venules. As a result, such methods should permit a finer grained localization of neuronal activity than does the BOLD signal alone, including when the BOLD signal is acquired during the application of simple diffusion weighting.
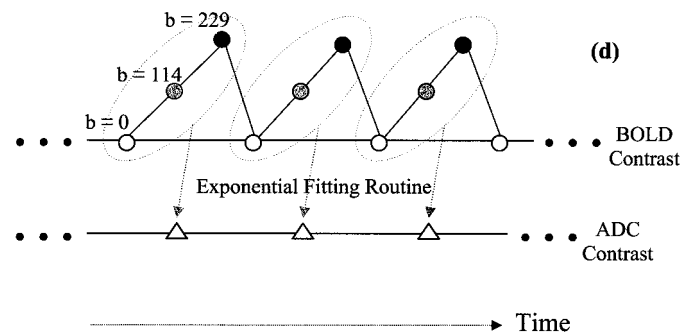

FIG. 2. Schematic illustration of the imaging strategy. The b factors of the IVIM/diffusion weighting were cycled every three scans (shown as circles with open circles at $b = 0$, gray circles at $b = 114$, and black circles at $b = 229$ s/mm²). The exponential fitting of the signal for each if these scan triplets (using Eq. 1) yielded an ADC estimate. Across the cycles, these then yielded the time course of the ADC values (shown as open triangles). The BOLD time courses (shown as open circles) are derived from those scans when $b = 0$ (i.e., when there was no IVIM weighting).
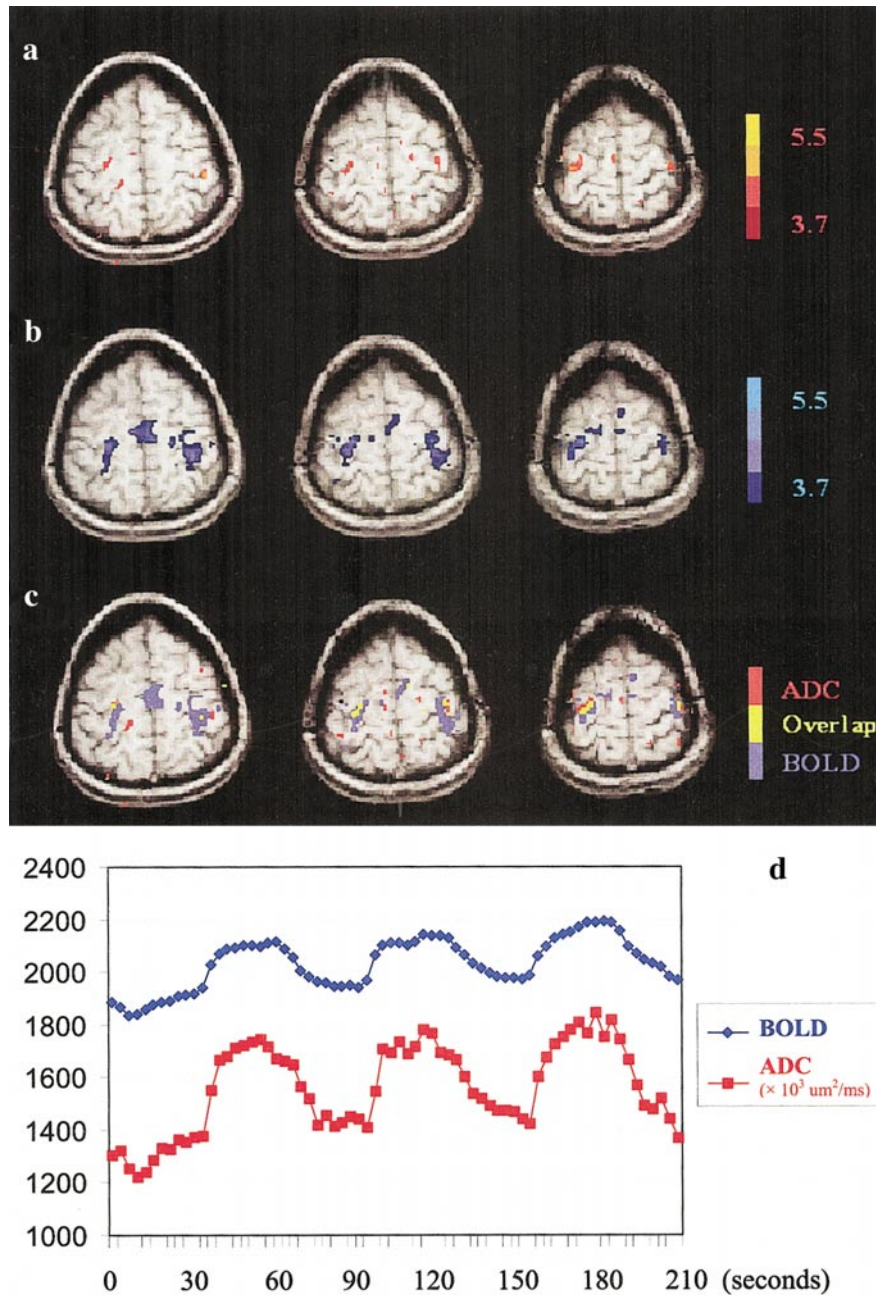
FIG. 3. Functional activation based on ADC, BOLD, and their activation overlap. Maps containing the positive activation using ADC contrast are shown for a representative subject in (a), with the maps containing positive BOLD activation shown in (b). Color bars indicate the z score thresholds. In (c), the spatial overlap between these two contrasts is shown in yellow to demonstrate the common activation of capillaries and the smallest vessels, thereby providing more accurate localization of the triggering neuronal activity. Averaged time courses from the two different contrast mechanisms are shown in (d), demonstrating the robustness of the activation. Also note that the percentage changes based on the ADC contrast are significantly larger than that of the BOLD contrast, consistent with the notion that blood flow increases more significantly than the blood oxygenation level.

METHODS

Six healthy volunteers (four males, two females, mean age 24 years) gave their written consent to participate as approved by the Institutional Review Board of Duke University Medical Center. The study was performed on a General Electric 4T whole-body MRI scanner (Milwaukee, WI) running on the LX platform.

To ensure spatially homogeneous attenuation of the vascular signal that was independent of the subject orientation in the scanner, isotropically weighted gra-

TABLE 1

Summary of the Numbers of Activated Pixels within the Regions Only Activated in the BOLD-Based Images, the Regions Activated in both the BOLD- and the ADC-Based Images, and the Regions Only Activated in the ADC-Based Images from the Six Participants

|	No. of BOLD-only pixels	No. of overlapping pixels	No. of ADC-only pixels
Subject 1	254	49	143
Subject 2	167	37	91
Subject 3[a]	154	26	73
Subject 4	128	29	83
Subject 5	95	19	49
Subject 6	73	13	47

[a] Shown in Fig. 3.

dient waveforms based on the design philosophy of the optimized isotropic diffusion weighting (Wong *et al.,* 1995) were generated. This method employs mutually orthogonal multilobe gradient waveforms on all three axes. The particular waveform used has a zero net flow moment in the *z* axis to allow analysis using a 2D random flow model. The isotropic weighting gradients were embedded into a gradient-recalled spiral imaging sequence (Ahn *et al.,* 1986; Meyer and Mocovski, 1987). The use of spiral acquisition permitted diffusion weighting and IVIM weighting without using excessively long echo times because the time between the excitation pulse and start of the spiral acquisition

could be fully exploited to accommodate the weighting gradients.

In order to visualize the dynamic changes in the mobility of the proton pools, as well as to assess contributions from different vessels, a temporally ramped IVIM weighting scheme was adopted. That is, the *b* factors were varied from one acquisition to the next, cyclically across three different *b*-factor values, so that the MR signals would be correspondingly attenuated in a cyclic fashion. Each experimental run contained many such cycles, and thus the cyclically varying attenuation would result in cyclic fluctuations of the signal at the frequency of the cyclic variation of the *b* factors (once per every three acquisitions). Since the acquisition rate was one acquisition per s, the temporal frequency of this cycling was one cycle every 3 s.

Functional neuronal activity was generated using a simple motor paradigm involving finger–thumb opposition. Subjects were instructed to bilaterally and sequentially tap their fingers and thumbs together for three and a half on/off cycles while the time-course volumes were acquired continuously. Each volume contained five axial slices of a 64 × 64 matrix at FOV of 24 cm through the motor cortex. A total of 210 volumes were acquired in each run of 3.5 min duration at a repetition time (TR) of 1 s and echo time (TE) of 50 ms. To eliminate in-flow contrast, the flip angle was set at 30°. Subjects were instructed through the scanner audio interface to rest for the first 30 s and then directed to alternate between finger tapping and rest at 30-s
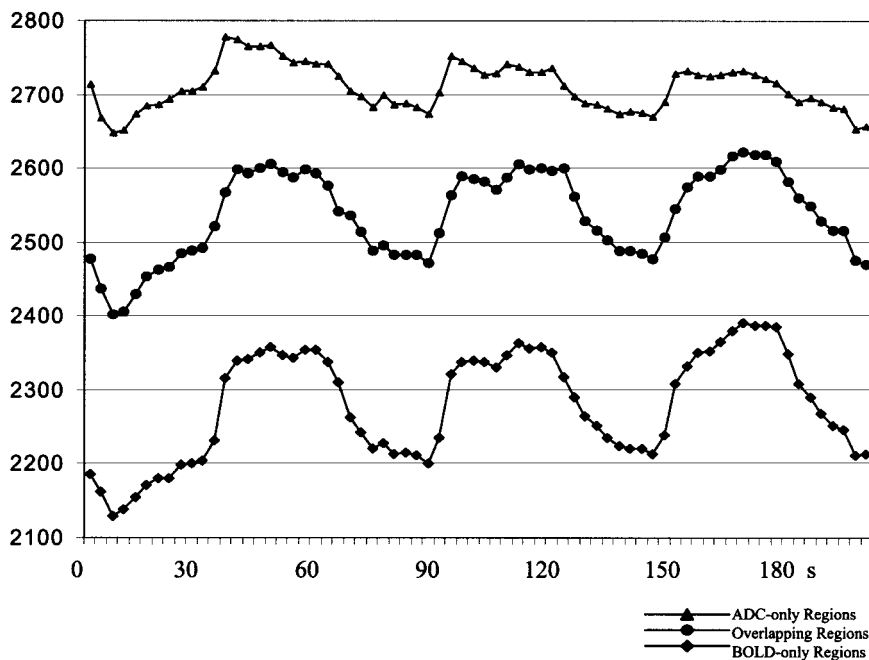
FIG. 4. Averaged BOLD time courses across the six subjects within the regions only activated in the BOLD-based images (shown in blue in Fig. 3c), the regions activated in both the BOLD- and the ADC-based images (shown in yellow in Fig. 3c), and the regions only activated in the ADC-based images (shown in red in Fig. 3c).

intervals. The three b factors for diffusion/IVIM weighting that were cyclically varied were 0, 114, and 229 s/mm^2. A total of 70 such cycles was acquired for each run. Four runs were acquired for each subject, the signals from which were then averaged together to gain statistical power. A set of high-resolution coplanar T1-weighted images was also acquired to serve as anatomical references.

Using Eq. (3), an exponential fitting algorithm was applied to the three signal values in each cycle of the averaged time courses for each voxel, yielding an estimated ADC for each cycle. Thus, across the cycles of the time course, this provided a dynamic time course of the ADCs; this is schematically illustrated in Fig. 2 as open triangles. Since these coefficients were varied within each run, the fitting procedure was not complicated by run-to-run variations as would have been the case if the different b factors were applied in different runs. This dynamic ADC time course therefore reflects the changing mobility of the proton pools, which is a result of the changing blood flow and perfusion (see discussion under the Theoretical Framework), from resting state to activation. A multiple regression algorithm was used to delineate statistically significant areas while effectively detrending any linear drifts in the time course. Since it has been suggested that the task-induced flow and perfusion changes mainly occur in the arteries, arterioles, capillaries, and venules (as veins do not experience much flow change with neural activation), the activated areas based on this ADC contrast mechanism would indicate mobility changes in these vessels.

The dynamic time-course images of the cycling IVIM weighting can also be sorted based on the b factors. That is, for each given b factor, a separate time course can be used to assess the effect of that IVIM weighting on the functional signal. Note that for the samples with a b factor of zero, the time course would be entirely based on the BOLD contrast, as illustrated in Fig. 2 (open circles). Activated pixels for this BOLD time course were found via the same multiple regression algorithm used in the ADC time course. Averaged time courses were also obtained within the activated areas. The resultant BOLD activation maps and time courses were used to compare with those obtained from the ADC contrast.

All images were acquired in the form of raw data (i.e., data before Fourier transformation), which were transported to an SGI Octane workstation (Mountain View, CA) for off-line reconstruction. A regridding algorithm in k-space was used to interpolate the spiral-sequence data to Cartesian space, and a standard fast Fourier transform was then performed to arrive at the final images. All images were concatenated into a volume format, and time courses were analyzed on a voxel-by-voxel basis.

RESULTS AND DISCUSSION

Both the ADC and the BOLD activation maps were acquired for each subject. Using the same statistical significance score ($Z > 3.7$), these maps all show significant pixels from both contrast mechanisms and small regions of overlap, shown as a summary in Table 1 by listing the numbers of the activated pixels from both maps and their overlap. To better illustrate the spatial representation of these regions, representative maps (from subject 3 in Table 1) of the ADC activation are shown in Fig. 3a with the statistical significance (Z scores) shown as color bars. To serve as a comparison, the BOLD activation maps using the identical processing method are shown in Fig. 3b, with the same statistical threshold selected as for the ADC maps. The ADC activation was then directly overlaid onto the BOLD activation for ease of comparison, shown in Fig. 3c. The ADC activations are shown in red, BOLD activation in blue, and their spatial overlap in yellow. Significant regions of nonoverlap can be seen between these two maps, indicating their differing sensitivity to hemodynamic changes. However, there is also significant overlap of the ADC and BOLD activations, indicating regions and thus neurovascular compartments for which both methods are sensitive. Since the ADC increases likely reflect mainly arterioles, capillaries, and venules, whereas the BOLD increases most likely reflect capillaries, venules, and veins, the overlap in Fig. 3c can be taken to reflect signal from the capillary and venule components. Such combined imaging of task-related activations provides better localization of the associated neuronal activities than methods that include other vascular components that are relatively more distant from the underlying neuronal activity. Averaged time courses within the activated areas for the ADC-based and BOLD-based maps are shown in Fig. 3d, demonstrating the robustness of the signal. The ADC contrast showed greater percentage changes than did the BOLD responses, consistent with the notion that the signal increases due more to blood flow changes than to oxygenation changes (Kim, 1995; Mandeville *et al.,* 1999; Hoge *et al.,* 1999).

To better understand the contributions of various vascular compartments to the functional signal, BOLD time courses were averaged across the six subjects within the three areas delineated in Fig. 3c, namely the regions activated only in the BOLD maps, the regions activated in both the BOLD and the ADC maps, and the regions only activated in the ADC maps. As demonstrated in Fig. 4, the smallest fractional changes during brain activation are shown in the BOLD time course from the ADC-only regions, intermediate changes are shown from the overlapping regions, and the largest changes are shown from the BOLD-only regions. This finding is consistent with the expectation that a gradation effect of the BOLD fractional changes would occur from the arteriole to the vein.
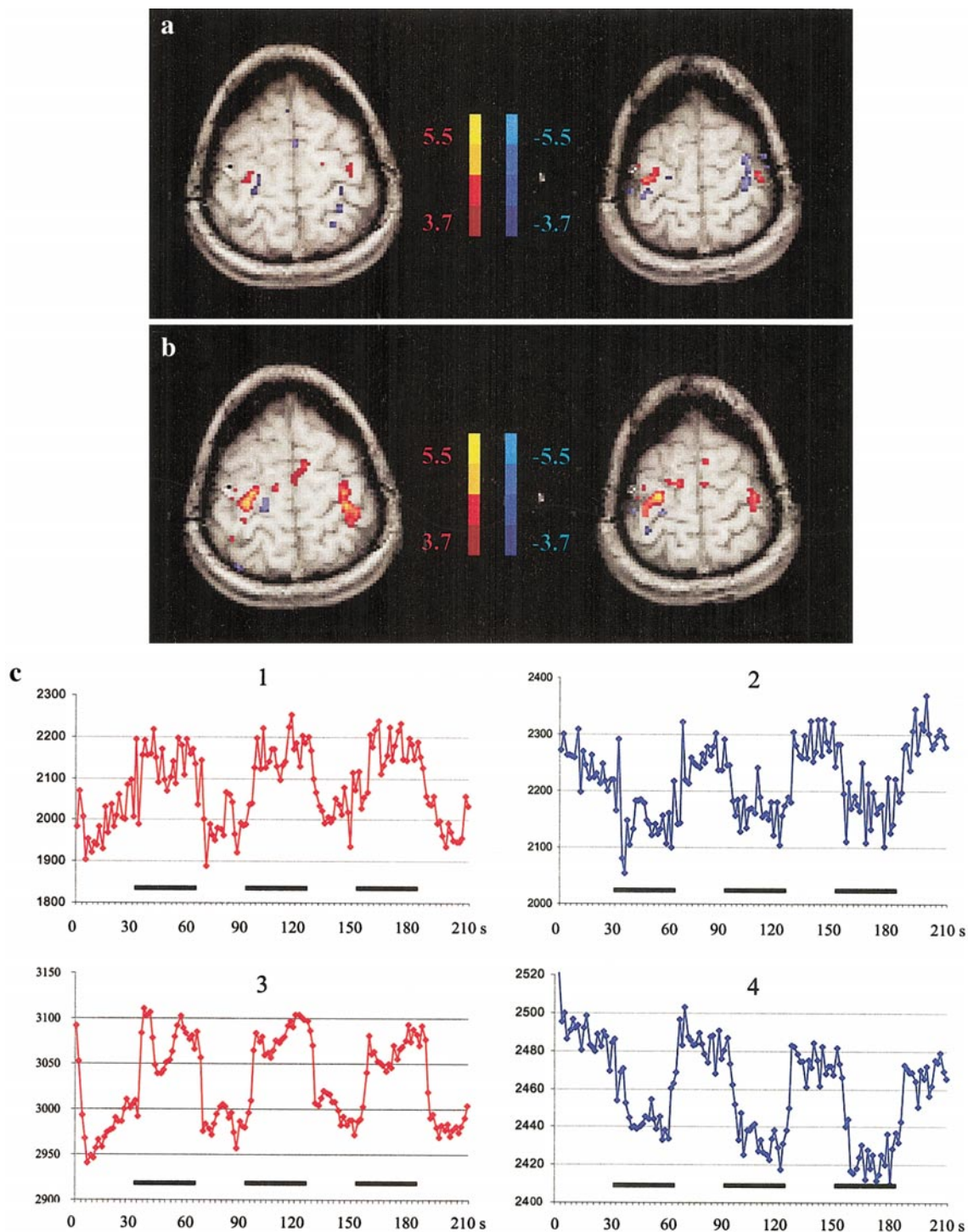
FIG. 5. Two representative slices of the ADC contrast including both positive and negative activations, shown in (a), compared with BOLD activations within the same slices, shown in (b). The lack of spatial overlap between the negative ADC activation and position positive BOLD activation confirms that the negative ADC activation is not of capillary or venule origin, as predicted by theory. Averaged time courses are shown in (c), respectively, for positive ADC (1), negative ADC (2), positive BOLD (3), and negative BOLD (4) activations. The horizontal bars indicate the time period during which the volunteers performed the finger-tapping task.

Also, it was found that the mean signal level from the ADC-only regions is the highest and that from the BOLD-only regions is the lowest, indicative of the overall concentration increase of the paramagnetic deoxyhemoglobin from the arterial to the venous side. These findings confirm our hypothesis on the origins of ADC activations.

In addition to increased ADC signal with neural activity, there were also significant negative activations (decreases) in the ADC contrast maps. Figure 5a shows two representative slices to illustrate these findings. These negative activations are likely from vessels that have higher velocities, such as large arterioles and small arteries, as predicted by Eq. (5) under the Theoretical Framework. This is supported by the finding that these negative ADC activations had little spatial overlap with BOLD activation (comparing Fig. 5a for ADC with Fig. 5b showing the BOLD maps). The respective time courses of the positive and negative activations are shown in Fig. 5c to demonstrate the clear temporal characteristics of the signal. There is, however, another possible mechanism for negative ADC contrast—that is, there truly was a decrease of blood flow to the local region. If this were the case, however, there should also have been a negative BOLD activation converging in the same spatial region, which did not occur in the images acquired in this study. Thus, the likely source for the observed negative ADC activations is the larger arterioles and small arteries. Nevertheless, it is important to note that if an area did show congruent negative ADC activation and BOLD activation, it would provide converging evidence that these small areas experience reduced blood flow.

CONCLUSIONS

We have demonstrated a new functional imaging method in which IVIM weighting could be used to generate an alternative image contrast based on the dynamic mobility changes, i.e., the apparent diffusion coefficient or ADC changes, of the intravascular proton pools. As suggested by the findings in this report, these changes likely originated from small arterial networks and capillaries. Thus, this method provides the capability of acquiring simultaneous and complementary contrasts based on blood-flow changes and BOLD signal changes during brain activation. The combination of the information from the two contrasts allows the delineation of capillary activation as the common activation, thereby providing a more precise localization of the underlying neuronal activities.

ACKNOWLEDGMENTS

REFERENCES

Ahn, C. B., Jim, J. H., and Cho, Z. H. 1986. High speed spiral-scan echo planar NMR imaging, *IEEE Trans. Med. Imag.* **MI-5:** 2–7.

Bandettini, P. A., Wong, E. C., Hinks, R. S., Tikofsky, R. S., and Hyde, J. S. 1992. Time course EPI of human brain function during task activation. *Magn. Reson. Med.* **25:** 390–397.

Belliveau, J. W., Kennedy, D. N., McKinstry, R. C., Buchbinder, B. R., Weisskoff, R. M., Cohen, M. S., Vevea, J. M., Brady, T. J., and Rosen, B. R. 1991. Functional mapping of the human visual cortex by magnetic resonance imaging. *Science* **254:** 716–719.

Boxerman, J. L., Bandettini, P. A., Kwong, K. K., Baker, J. R., Davis, T. L., Rosen, B. R., and Weisskoff, R. M. 1995. The intravascular contribution to fMRI signal change: Monte Carlo modeling and diffusion weighted studies *in vivo. Magn. Reson. Med.* **34:** 4–10.

Darquie, A., Clark, C. A., Van de Moortele, P. F., and Le Bihan, D. 1999. Comparison of BOLD and IVIM event-related fMRI. *Proc. ISMRM* **7:** 447.

Darquie, A., Poline, J. B., Poupon, C., Saint-Jalmes, H., and Le Bihan, D. 2001. Transient decrease in water diffusion observed in human occipital cortex during visual stimulation. *Proc. Natl. Acad. Sci. USA* **98:** 9391–9395.

Does, M. D., Zhong, J., and Gore, J. C. 1999. In vivo measurement of ADC change due to intravascular susceptibility variation. *Magn. Reson. Med.* **41:** 236–240.

Guyton, A. C., and Hall, J. E. 2000. *Textbook of Medical Physiology,* 10th ed., Saunders, Philadelphia.

Hoge, R. D., Atkinson, J., Gill, B., Crelier, G. R., Marrett, S., and Pike, G. B. 1999. Investigation of BOLD signal dependence on cerebral flow and oxygen consumption: The deoxyhemoglobin dilution model. *Magn. Reson. Med.* **42:** 849–863.

Kim, S.-G. 1995. Quantification of relative cerebral blood flow changes by flow-sensitive alternating inversion recovery (FAIR) technique: Application to functional mapping. *Magn. Reson. Med.* **34:** 293–301.

Kwong, K. K., Belliveau, J. W., Chesler, D. A., Goldberg, I. E., Weisskoff, R. M., Poncelet, B. P., Kennedy, D. N., Hoppel, B. E., Cohen, M. S., Turner, R., Cheng, H. M., Brady, T. J., and Rosen, B. R. 1992. Dynamic magnetic resonance imaging of human brain activity during primary sensory stimulation. *Proc. Natl. Acad. Sci. USA* **89:** 5675–5679.

Le Bihan, D., Breton, E., Lallemand, D., Grenier, P., Cabanis, E., and Laval-Jeantet, M. 1986. MR imaging of intravoxel incoherent motions: Application to diffusion and perfusion in neurologic disorders. *Radiology* **161:** 401–407.

Le Bihan, D., and Turner, R. 1992. The capillary network: A link between IVIM and classical perfusion. *Magn. Reson. Med.* **27:** 171–178.

Le Bihan, D., Breton, E., Lallemand, D., Aubin, M.-L., Vignaud, J., and Laval-Jeantet, M. 1988. Separation of diffusion and perfusion in intravoxel incoherent motion MR imaging. *Radiology* **168:** 497–505.

Mandeville, J. B., Marota, J. J. A., Ayata, C., Moskowitz, M. A., Weisskoff, R. M., and Rosen, B. R. 1999. MRI measurement of the temporal evolution of relative CMRO2 during rate forepaw stimulation. *Magn. Reson. Med.* **42:** 944–951.

Menon, R., Ogawa, S., Tank, D. W., and Ugurbil, K. 1993. 4 Tesla gradient recalled echo characteristics of photic stimulation-induced signal changes in the human primary visual cortex. *Magn. Reson. Med.* **30:** 380–386.

Meyer, C. H., and Mocovski, A. 1987. Square spiral fast chemical shift imaging. *Magn. Reson. Imag.* **5:** 519.

Ogawa, S., Tank, D. W., Menon, R., Ellerman, J. M., Kim, S. G., Merkle, H., and Ugurbil, K. 1992. Intrinsic signal change accompanying sensory stimulation: Functional brain mapping with mag-

netic resonance imaging. *Proc. Natl. Acad. Sci. USA* **89:** 5951–5955.

Ogawa, S., Menon, R. S., Tank, D. W., Kim, S. G., Merkle, H., Ellerman, J. M., and Ugurbil, K. 1993. Functional brain mapping by blood oxygenation level dependent contrast magnetic resonance imaging. *Biophys. J.* **64:** 803–812.

Song, A. W., Wong, E. C., Tan, S. G., and Hyde, J. S. 1996. Diffusion weighted FMRI at 1.5 T. *Magn. Reson. Med.* **35:** 155–158.

Song, A. W., and Popp, C. A. 1998. fMRI using ADC contrast. *Proc. ISMRM* **6:** 1438.

Song, A. W., Woldorff, M., Fichtenholtz, H., Mangun, G. R., and McCarthy, G. 2000. Flow-sensitive alternating diffusion-weighting effect: A direct method to distinguish vascular and parenchymal contributions to brain fMRI signal. *Proc. ISMRM* **9:** 1169.

Torrey, H. C. 1956. Bloch equation with diffusion terms. *Phys. Rev.* **104**(3): 563–566.

Turner, R., Jezzard, P., Wen, H., Kwong, K. K., LeBihan, D., Zeffiro, T., and Balaban, R. S. 1993. Functional mapping of the human visual cortex at 4 and 1.5 Tesla using deoxygenated contrast EPI. *Magn. Reson. Med.* **29:** 277–279.

Wong, E. C., Cox, R. W., and Song, A. W. 1995. Optimized isotropic diffusion weighting. *Magn. Reson. Med.* **34:** 139–143.

Zhong, J., Kennan, R. P., Fulbright, R. K., and Gore, J. C. 1998. Quantification of intravascular and extravascular contributions to BOLD effects induced by alteration in oxygenation or intravascular contrast agents. *Magn. Reson. Med.* **40**(4): 526–536.

Zhong, J., Kennan, R. P., and Gore, J. C. 1991. Effects of susceptibility variations on NMR measurements of diffusion. *J. Magn. Reson.* **95:** 267–280.